REVISTA MATÉRIA V.30
ISSN 1517-7076 articles e20250153, 2025

Numerical analysis of stress field modification in rails to evaluate the minimum specimen dimensions for FBW process's residual stress measurements

Matheus Miranda Duarte de Castro[1], Leonardo Dantas Rodrigues[1]

[1]Universidade Federal do Pará, Programa de Pós-Graduação em Engenharia Mecânica. Belém, PA, Brasil.
e-mail: matheus_98castro@hotmail.com, leodr@ufpa.br

ABSTRACT

This study aimed to determine the optimal specimen size using a finite element model, minimizing dimensions for better logistical efficiency while maintaining the stress field's integrity. The methodology consisted of simulating a cutting process on a specimen, where the only mechanical load applied was the residual stress resulting from the flash butt welding (FBW) process, which is the most commonly used method for joining rail segments. Consequently, any variation observed in the residual stresses was attributed to a redistribution caused by material removal. The cutting process was simulated by sequentially removing elements with the element death feature, replicating vertical cutting conditions. Cutting distances ranged from 200 mm to 25 mm from the weld interface to identify the optimal distance preserving stress field setup. The results showed that stress variation increased as the cut approached the weld interface. A cut at 25 mm caused significant changes in the stress field, with an average difference of 89%, while a 125 mm cut resulted in a smaller 3% variation at measured points. These findings highlight the importance of selecting appropriate specimen sizes to ensure accurate mechanical testing and residual stress analysis in railway applications.

Keywords: Residual stresses analysis, Stress field modification, Finite element method, Rail integrity.

1. INTRODUCTION

There are two main types of rail welding processes: Flash Butt Welding (FBW) and aluminothermic welding. However, the use of continuous welded rails (CWR) through the FBW process accounts for approximately 80% of rail welds worldwide due to its superior quality [1]. In this process, an electric current is applied between the end of the rails that are being joined. This contact electrification and flash generation are repeated several times until a molten metal layer, formed by the Joule effect caused by the electrical current, covers the entire joint surface. Then, through the rapid advancement of the rails and the applied pressure, the welded joint is formed [2]. As in other welding processes, recent measurements conducted by [3] and [4] have shown that FBW can generate high residual stress values in rails, especially in the web region. Several studies, such as [5], [6], and [7], highlight the significant effect these high stresses can have on reducing the service life of rails.

Therefore, in recent decades, many researchers have dedicated efforts to experimental and numerical studies to evaluate the residual stresses generated in this process and to establish welding parameter changes and/or post-welding treatments that could help reduce these stresses. In [8], residual stresses in the FBW process were analyzed, considering phase transformation to identify critical locations and optimize welding parameters to reduce tensile stresses. In [9], X-ray diffraction revealed that the welding process, along with additional steps such as heat treatment and straightening, contributed to the increase in residual stresses in rails. The objective of [10] was to investigate the fatigue characteristics of CWR and the effect of residual stress on fatigue-ratchetting interaction. Due to the complexity of these models, even numerical analyses must be validated by experimental data.

Performing a consistent number of experimental residual stress measurements in rails, with greater statistical validity, faces significant logistical challenges, particularly in the preparation, transportation, and handling of specimens. The high weight of rails complicates large-scale transportation and storage in research institutions, where they are typically evaluated. Additionally, handling and preparing samples for measurements may become complex depending on the dimensions of the test specimens. For that reason, specimens with reduced dimensions can help overcome these challenges and allow for a larger number of experimental

Corresponding Author: Leonardo Dantas Rodrigues Received on 17/02/2025 Accepted on 27/05/2025

DOI: https://doi.org/10.1590/1517-7076-RMAT-2025-0153

assessments. However, cutting the welded samples to smaller dimensions must not alter the stress state in the weld region that is intended to be evaluated.

In this study, a numerical model was created using the finite element method to simulate the modification of residual stresses caused by cuts at different distances from the fusion line (FL). For this, a residual stress state generated by the FBW process, obtained from a previous model developed in this same project, was used as input data, further detailed in [11]. It should be added that results similar to those obtained in reference [11] and used as reference and input data in the models of this article can also be found in the literature, such as in [12], [13] and [14].

The model's results were compared with some experimental measurements conducted on specimens with lengths of 2 m (136 kg) and 0.35 m (26,8 kg).

2. MATERIALS AND METHODS

The focus of this study was numerical modeling. However, to help corroborate the obtained results, residual stress measurement results are also presented for AREMA 136 RE rails welded using the FBW method, some with a length of 2 m and others with 0.35 m. Table 1 shows some of the characteristics of these specimens.

2.1. Experimental methodology

Measurements were taken at four points on each specimen, one at the FL on the head, foot, and web, and one at approximately 22 mm from the FL on the web (HAZ boundary). Figure 1 shows a schematic of measurement points. This distance is based on the actual size of the heat-affected zone, with an average value of approximately 44 mm. The assumed value is corroborated by some papers in the literature for rails similar to those evaluated in this work, such as in [15].

Table 1: List of specimens and their available relevant characteristics.

SPECIMEN	MANUFACTURER	LENGTH (m)	YIELD STRENGTH (MPa)	ULTIMATE STRENGTH (MPa)	ELONGATION (%)	HARDNESS (HB)
P1	Nippon Steel	2	830	1290	14	331–388
P2	Nippon Steel	2	830	1290	14	331–388
P3	Nippon Steel	2	830	1290	14	331–388
P4	Nippon Steel	0.35	830	1290	14	331–388
P5	Arcelormittal	0.35	760	1179	10	370
P6	Arcelormittal	0.35	760	1179	10	370

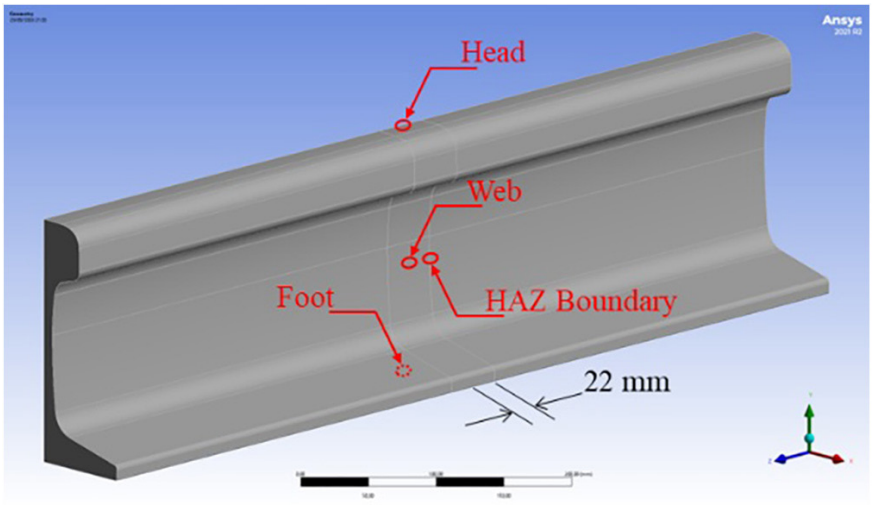

Figure 1: Location of the measurement points distributed along the rail.

Extensometric techniques are widely used for experimental residual stress analysis due to their high reliability [16]. The most used among these is the hole-drilling method, which was performed in this study following ASTM E837-13 guidelines [17]. Figure 2a shows the basic setup for the procedure. From this apparatus, the guide channel, magnifying lens, and pneumatic drill can be highlighted. The B-type rosettes used, with an example shown in Figure 2b, were designed according to ASTM E837-13 specifications and had a hole diameter of approximately 1.6 mm.

In summary, the measurement procedure consists of drilling a hole 1 mm deep in 20 increments of 0.05 mm each. At each increment, the strains recorded by the three strain gauges in the rosette are documented. Upon completion of the measurements, two distinct mathematical treatments can be employed to derive the stresses: one for cases where strains vary linearly with depth and another for non-linear variations. In the conducted measurements, the behavior was predominantly linear; thus, the linear method was utilized, applying the strain-stress correlation coefficients for uniform conditions.

2.2. Material parameters and properties used in the modeling

The rail used as the study reference was a premium grade rail from Nippon Steel, AREMA 136 RE model, as standardized by [18], similar to the work carried out by [11], with composition and mechanical properties shown in Table 2 and the profile shown in Figure 3.

Based on the material properties provided by the manufacturer, properties such as yield strength, ultimate tensile strength, Young modulus, among others, were input in the model. For the other properties, the default values of a structural steel available in the Ansys library were used.

2.3. Construction of the model's three-dimensional geometry

A three-dimensional object was then constructed using SpaceClaim, one of the design tools available in the Ansys suite, with dimensions and characteristics similar to those used by [11], with the difference that the new object uses ¼ symmetry, having half the length of the original object. This proceeding was adopted considering the symmetrical nature of the model's boundary conditions, which allowed a greater mesh refinement without increasing the total number of elements, contributing to a reduced processing time. Additionally, the new body includes 20 intermediate bodies of 5 mm in length, sectioning the rail along the vertical axis, as shown in Figure 4a. These bodies were used as a tool for the sequential removal of material to simulate a complete cut in the rail.

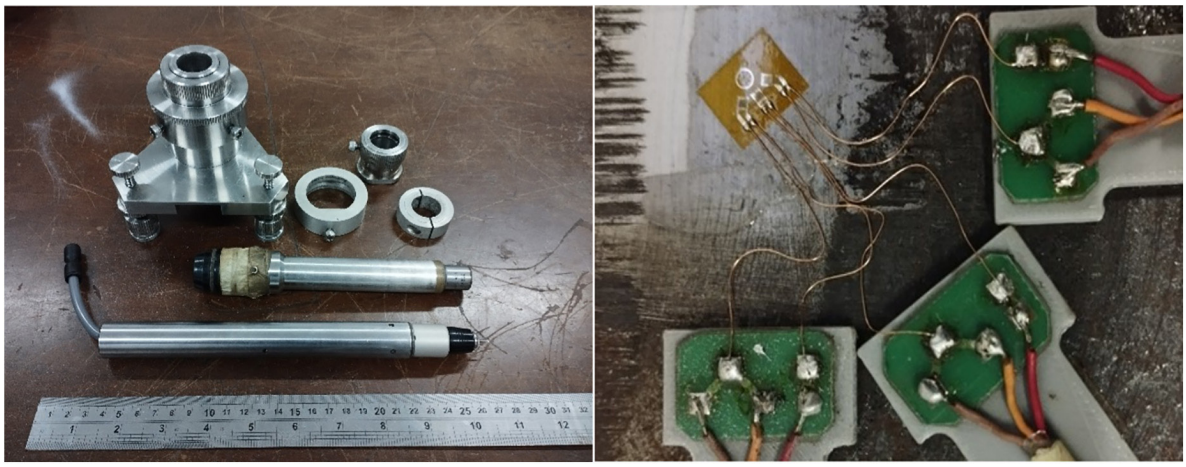

Figure 2: a) Set of components of the drilling apparatus; b) Type-B rosettes bonded and wired on the rail's web surface.

Table 2: Rail composition and mechanical properties.

C (%)	Si (%)	Mn (%)	P (%)	S (%)	YIELD STRENGTH (MPa)	ULTIMATE STRENGTH (MPa)	ELONGATION (%)	HARDNESS (HB)
0.81	0.30	1.04	0.02	0.02	830	1290	14	331–388

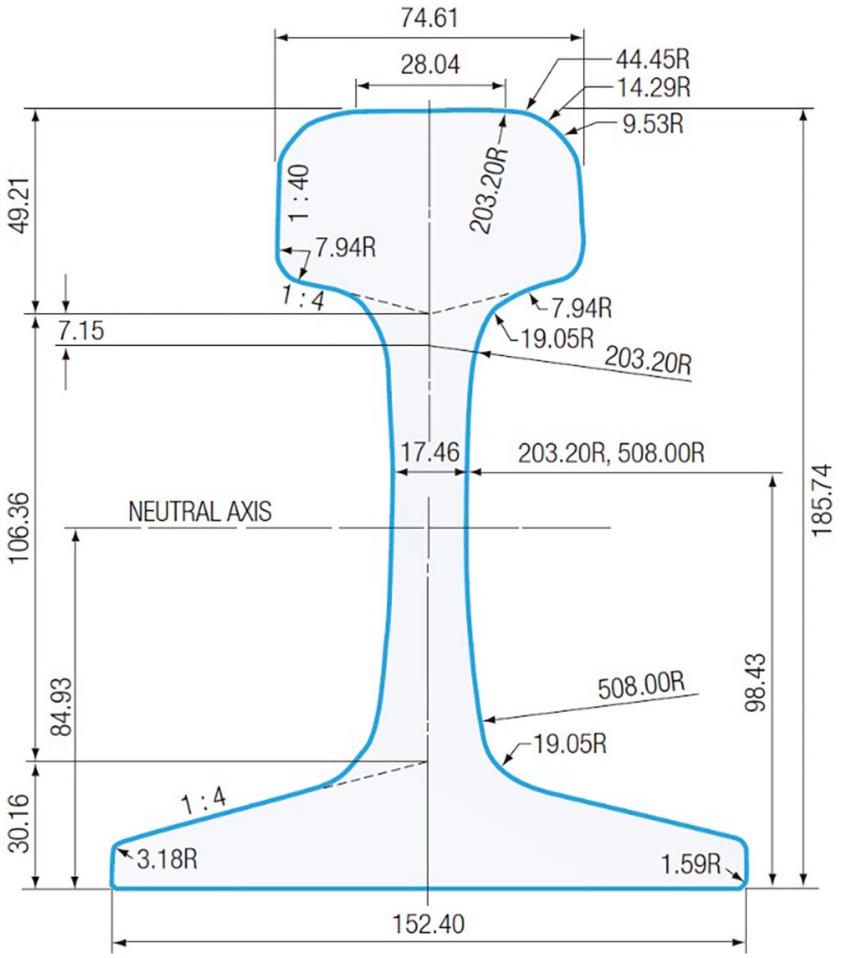

Figure 3: AREMA 136 RE rail profile, dimensions in millimeters.

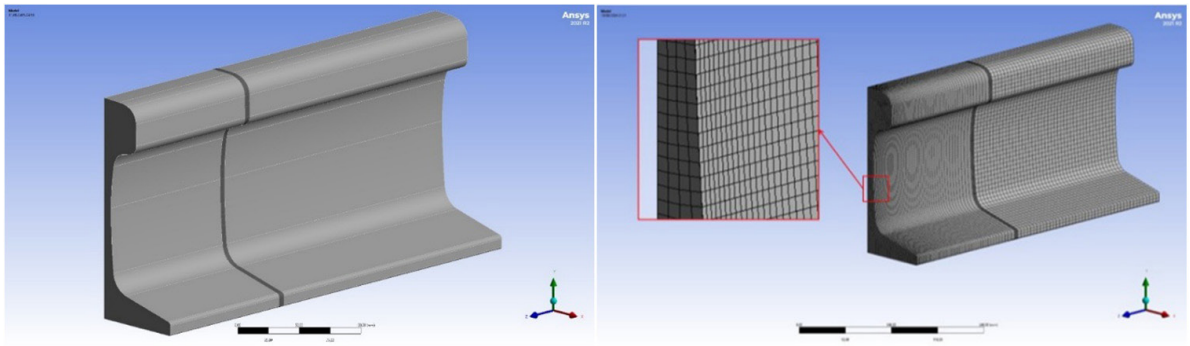

Figure 4: a) Three-dimensional object constructed for rail cutting simulation and b) Finite element mesh constructed for the rail cutting simulation.

The material parameters and properties of the model were configured similarly to those defined by [11]. The mesh configuration for each cutting distance had a different number of SOLID186 elements, ranging from 7323 elements in the 25 mm model to 20711 elements in the 200 mm model. This kind of element is a higher-order 3D solid element defined by 20 nodes with three degrees of freedom per node. It supports large deflections and has high deformation capability. The mesh constructed for each model, as shown in Figure 4b, was configured and refined so that in the region of interest, near the weld, there is a higher refinement characterized by 0.5 mm-sided elements, and as the distance from this interface increases, the element size progressively increases until the element reaches 10 mm length while still maintaining the necessary quality.

To determine the appropriate element size, a mesh convergence analysis was performed to ensure the accuracy and reliability of the obtained results. Successive mesh refinements were conducted, and the results at a selected point were monitored until the values of interest stabilized, indicating a solution convergence. It was found that from an element size of 0.5 mm onward, the results became virtually unchanged with further refinements. Therefore, this was considered the ideal mesh size to adequately represent the behavior of the analyzed system. The evolution of the results throughout the refinements and the identification of the convergence point can be seen in Figure 5, corresponding to the cutting model at 200 mm from the FL. This size was then considered for all other cutting distances.

2.4. Boundary conditions

The stress state from the P4 specimen's FBW welding model in [11] was used as input for the cutting model (see Figure 6). The analysis in [11] was divided into two stages: thermal and mechanical simulations. Boundary conditions included a transient thermal analysis with localized heat generation in the heat-affected zone (HAZ)—100 kW/mm^3 in the head/foot and 112 kW/mm^3 in the web—along with a surface heat flux of 1200 W, convection with geometry-dependent coefficients, and thermal radiation with emissivity of 0.75. In the mechanical stage, the thermal gradients were applied as loads, with displacement constraints at one end of the rail to prevent rigid body movement. Different mechanical properties were assigned for heating and cooling phases,

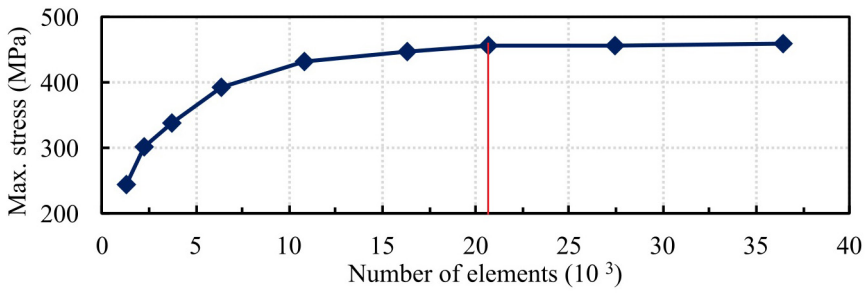

Figure 5: Mesh convergence analysis used in the 200 mm model.

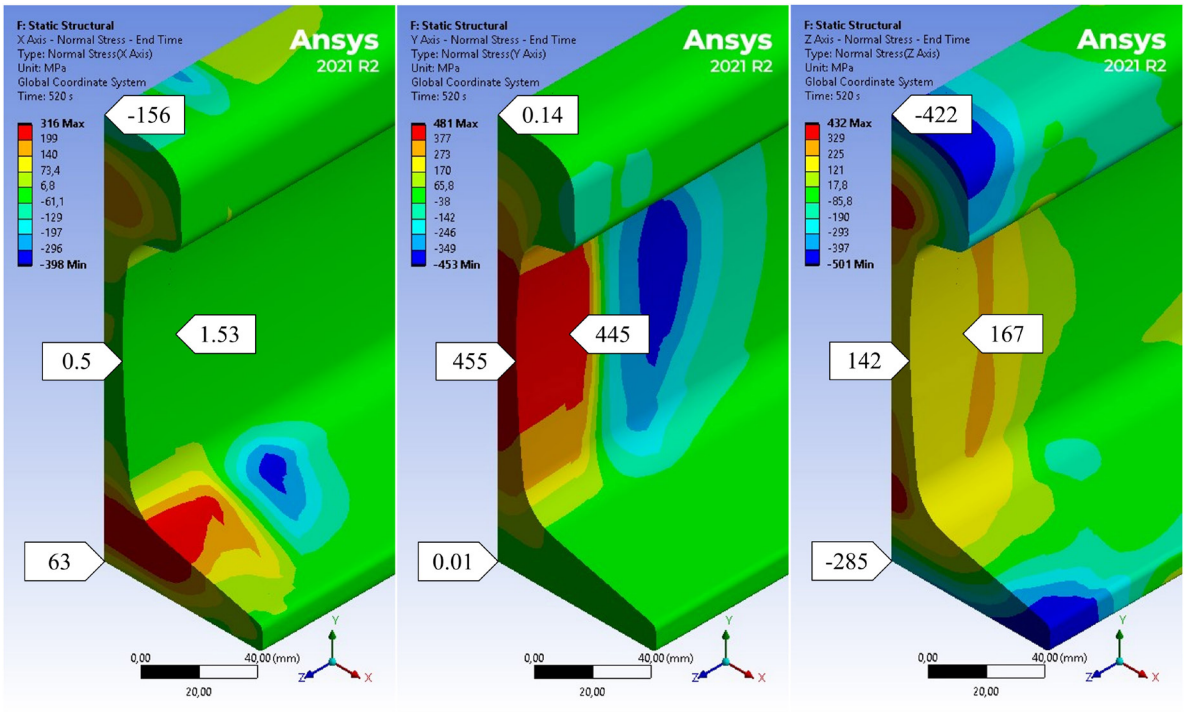

Figure 6: a) Transverse (σ_x); b) vertical (σ_y); c) longitudinal (σ_z) residual stress state imported as initial state for the model, values in MPa.

adjusted by literature [12], [13] and [14] to reflect microstructural changes. Additionally, a displacement constraint was applied to one of the lateral vertices of the rail. This displacement acted as an anchor for the model, preventing rigid body motion. The chosen location for this boundary condition was in a region sufficiently distant from the welding zone to avoid any influence on the magnitude of residual stresses in the weld region after cutting due to contact effects or proximity to applied loads, ensuring that all results were exclusively derived from the stress modification caused by the material removal.

For the sequential removal of the bodies, the model was divided into 20 steps of 1 second each, with one intermediate body being removed at each step, starting from the upper end of the rail. This removal is carried out using the element birth and death tool. This procedure was repeated by varying the cutting distances from 25 mm to 200 mm measured from the FL, aiming to identify an optimal distance that would maintain the integrity of the stress field of interest. Figure 7 illustrates the overall arrangement of the cutting conditions used in the numerical model, as well as the reference measurement points.

3. RESULTS OF EXPERIMENTAL TRIALS

On rails P1 and P2, no measurements were made on the foot. Tables 3, 4 and 5 show the results of measurements on the specimens in the positions indicated in Figure 1 in the transverse (σ_x), vertical (σ_y) and longitudinal (σ_z) directions, respectively.

The presented results are consistent with the stress behaviors reported in the literature, such as in [3] and [4]. Specifically, they show compressive longitudinal stresses in the head and base and tensile stresses in the web, as well as tractive vertical stresses in the web, both in the FL and HAZ boundary regions.

However, the primary purpose of the experimental results is to demonstrate that the magnitudes of residual stresses in the web region do not show significant differences between the 2 m and 0.35 m specimens. In this

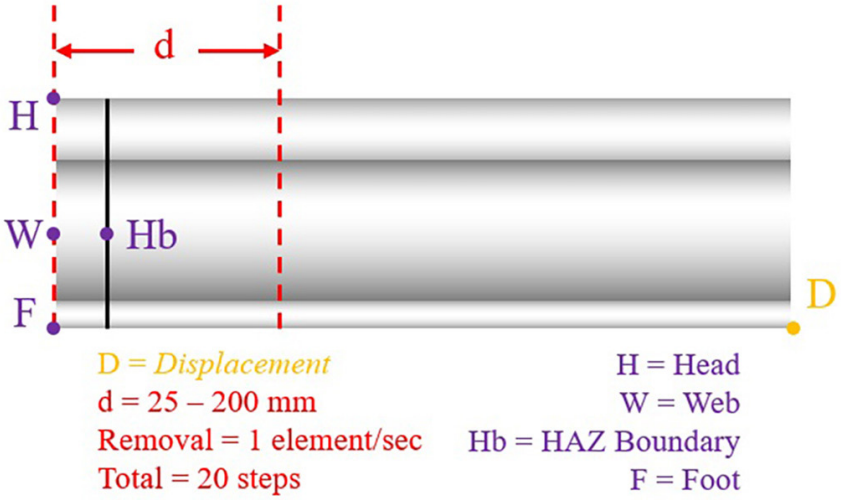

Figure 7: General cutting conditions arrangement used in the numerical model.

Table 3: Transverse residual stress (σ_x) results in the measured samples (MPa).

SPECIMEN	HEAD	WEB*	HAZ BOUNDARY*	FOOT
P1 (2 m)	–130	–	–	–
P2 (2 m)	–96	–	–	–
P3 (2 m)	–44	–	–	62
P4 (0.35 m)	–342	–	–	700,94
P5 (0.35 m)	–229,37	–	–	185
P6 (0.35 m)	42,03	–	–	59,89

* Residual stress in the transverse direction (σ_x) is negligible at these points.

Table 4: Vertical residual stress (σ_y) results in the measured samples (MPa).

SPECIMEN	HEAD*	WEB	HAZ BOUNDARY	FOOT*
P1 (2 m)	–	204	320	–
P2 (2 m)	–	364	261	–
P3 (2 m)	–	417	325	–
P4 (0.35 m)	–	295,55	286,41	–
P5 (0.35 m)	–	226,58	292,19	–
P6 (0.35 m)	–	51,52	246	–

* Residual stress variations in the vertical direction (σ_y) are negligible at these points.

Table 5: Longitudinal residual stress (σ_z) results in the measured samples (MPa).

SPECIMEN	HEAD	WEB	HAZ BOUNDARY	FOOT
P1(2 m)	–202	180	162,5	–
P2 (2 m)	–281	307	163	–
P3 (2 m)	–132	521,5	168	–9
P4 (0.35 m)	–218	138,13	197,09	261,78
P5 (0.35 m)	–242,88	247,25	178,85	101
P6 (0.35 m)	–121,52	53,49	262	42,31

regard, most specimens showed similar results. This is an important indication that the residual stresses in the weld region were not significantly altered in the specimens cut to 0.35 m in length.

4. RESULTS OF NUMERICAL MODELS

Regarding the numerical model results, for all cut distances, the solution converged in approximately 2 hours and 40 minutes of numerical processing. As expected, for cuts made very close to the fusion line, the stress modification effect caused by the cut was more prominent, as observed in Figure 8 and 9, which illustrates the stress state after cuts made at 25 mm and 50 mm from the FL, the effect of the cut's proximity on the magnitude of residual stresses in the weld region is noticeable when compared to the initial state shown in Figure 6. It is important to highlight that a variation greater than 100% indicates that, in addition to completely relieving the stresses at that point, the cut also caused an inversion in the stress behavior. On the other hand, a negative variation value indicates that there was no stress decrease at that point, but rather an increase in stresses of the same nature.

Figures 10a and 10b illustrate the variation of residual stresses in the transverse direction (σ_x) as the cutting zone moves away from the FL. In the rail head, a significant relief of 88% was observed at a distance of 25 mm, decreasing to 24% at 50 mm, and tending toward zero beyond 100 mm. In the rail foot, the closest cut resulted in a –58% increase, followed by stress increase of –36.5% at 50 mm, with a tendency to remain below 5% after 150 mm. For the web and the HAZ boundary, the stress variation caused by the cuts was negligible in this direction.

Figures 11a and 11b show the variation of residual stresses in the vertical direction (σ_y) as the cutting zone moves away from the FL. The stress behavior during the cutting simulations exhibited significant alteration in this direction, with similar patterns for the web and the HAZ boundary, showing reductions of approximately 102%, indicating strong reduction with stress inversion, for cuts at 25 mm from the FL. At 50 mm, the reduction was around 60%, while beyond 75 mm, the reductions were less than 10%, with negligible results after 100 mm. For the rail head and foot, the stress modification in this direction was insignificant for the final values.

Figures 12a and 12b show the variation of residual stresses in the longitudinal direction (σ_z). At 25 mm from the FL, the highest variation recorded was 110% at the HAZ boundary, followed by 99.9% in the web, 95% in the rail head, and 85% in the base. At 50 mm, there was a significant reduction and stress inversion in the web and the HAZ boundary, with 152% and 135%, respectively, along with reductions of approximately 78% and

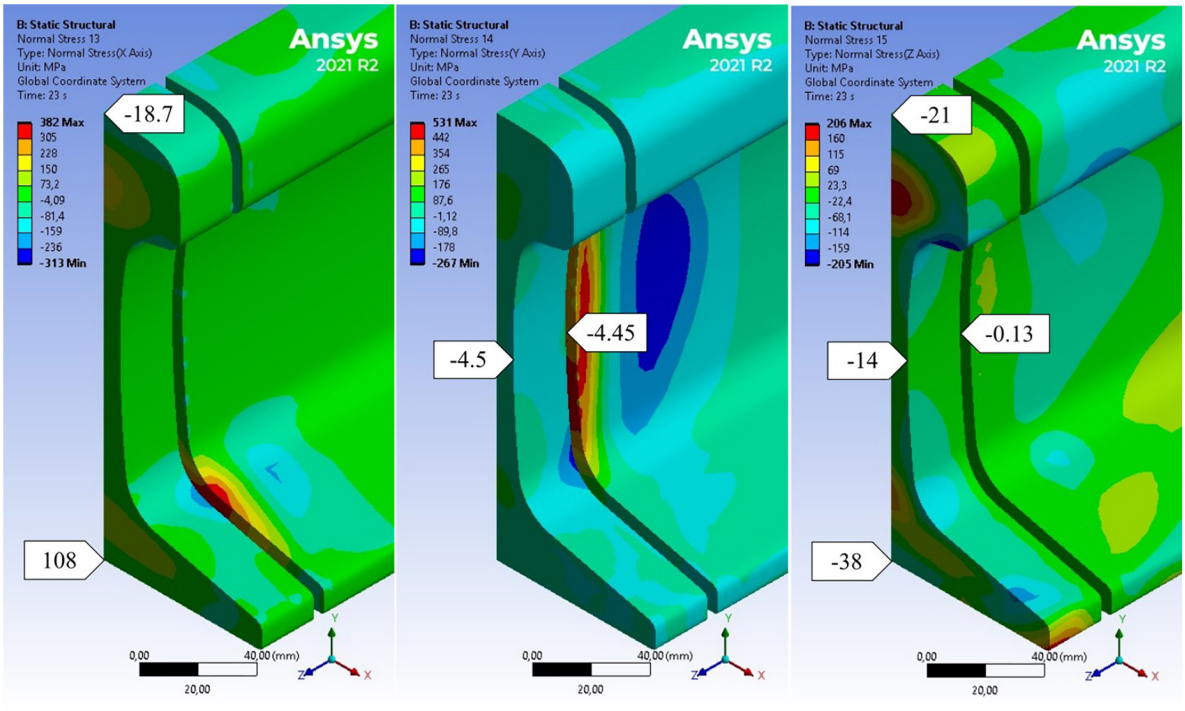

Figure 8: Residual stress state: a) transverse (σ_x), b) vertical (σ_y), and c) longitudinal (σ_z), in MPa, after cutting at 25 mm from the fusion line.

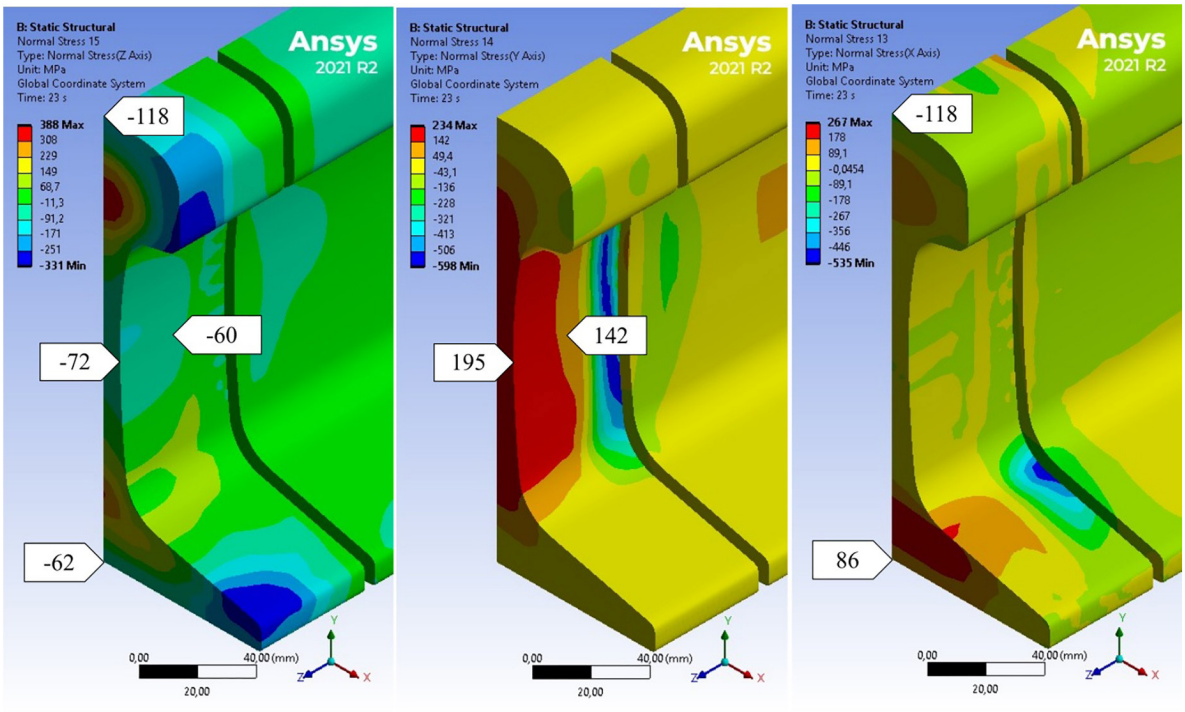

Figure 9: Residual stress state: a) transverse (σ_x), b) vertical (σ_y), and c) longitudinal (σ_z), in MPa, after cutting at 50 mm from the fusion line.

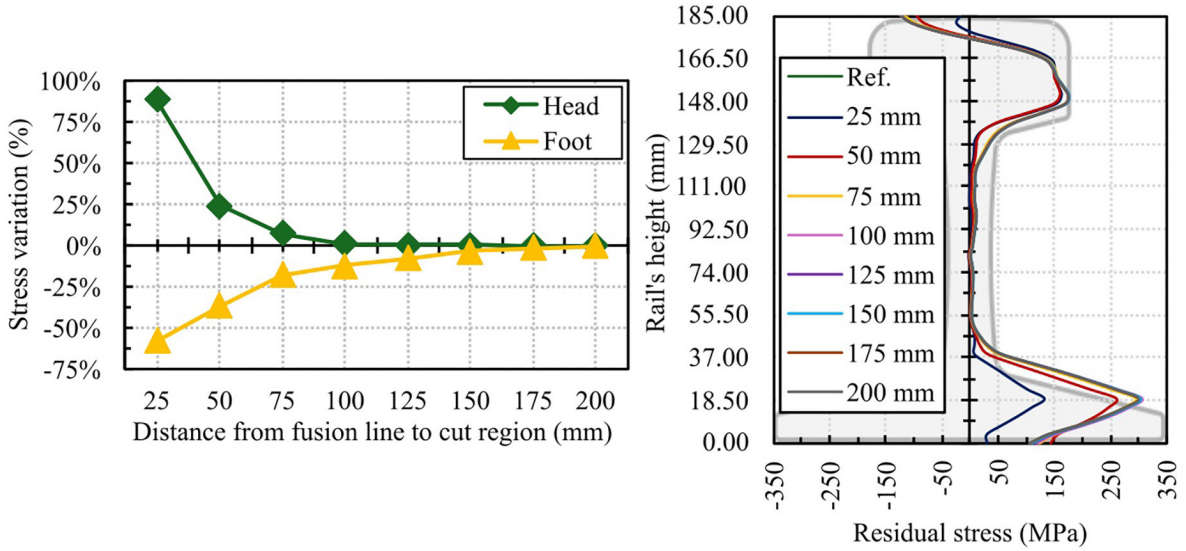

Figure 10: Transverse residual stress (σ_x) variation a) in the measured positions and b) along the rail's height at the FL.

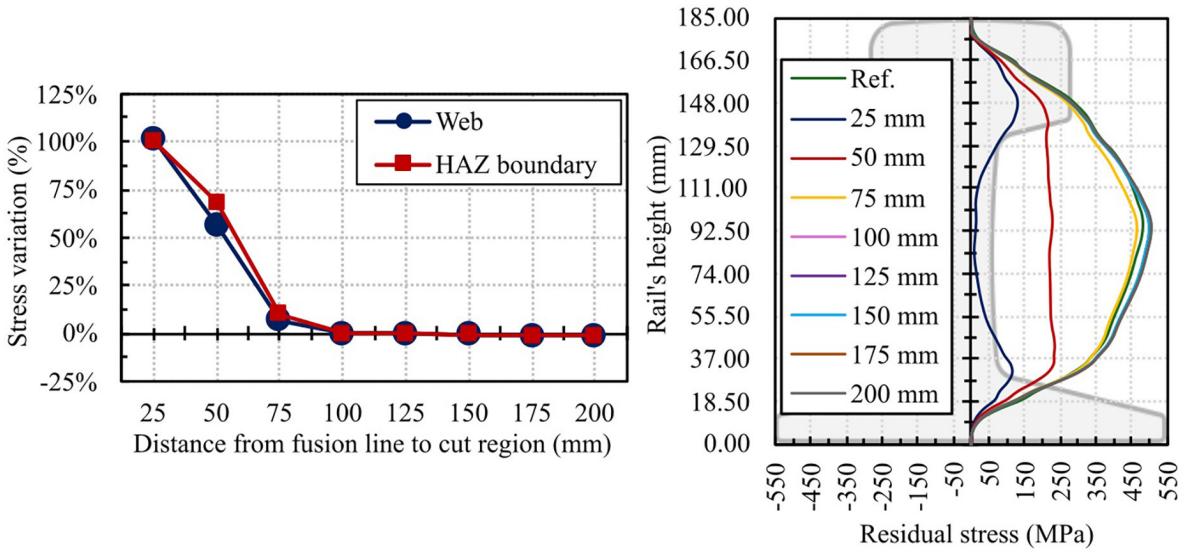

Figure 11: Vertical residual stress (σ_y) variation a) in the measured positions and b) along the rail's height at the FL.

72% in the base and rail head. Beyond 100 mm from the fusion line, the cutting effects caused interference of less than 5% at all four measurement points.

The graphs in Figures 10 to 12 show that there is no significant variation in stress either along the neutral axis or at the HAZ boundary for cuts made from a distance of 150 mm from the fusion line. This information is qualitatively supported by the experimental results presented in Tables 3 to 5, which contain residual stress measurements in specimens with total lengths of 2 m and 0.35 m, both with the fusion line at the center. Although the specimens are not entirely identical, the experimental results indicate that the specimen size did not significantly affect the residual stresses in the zone of interest.

5. CONCLUSIONS

Based on the results found, it can be said that the general trend is for a reduction in the magnitude of the stresses as the cuts approach the fusion line, as expected. The exception was the transverse stresses in the skate, which increased as the cuts approached. There was also an exceptional behavior in the longitudinal stresses in the web

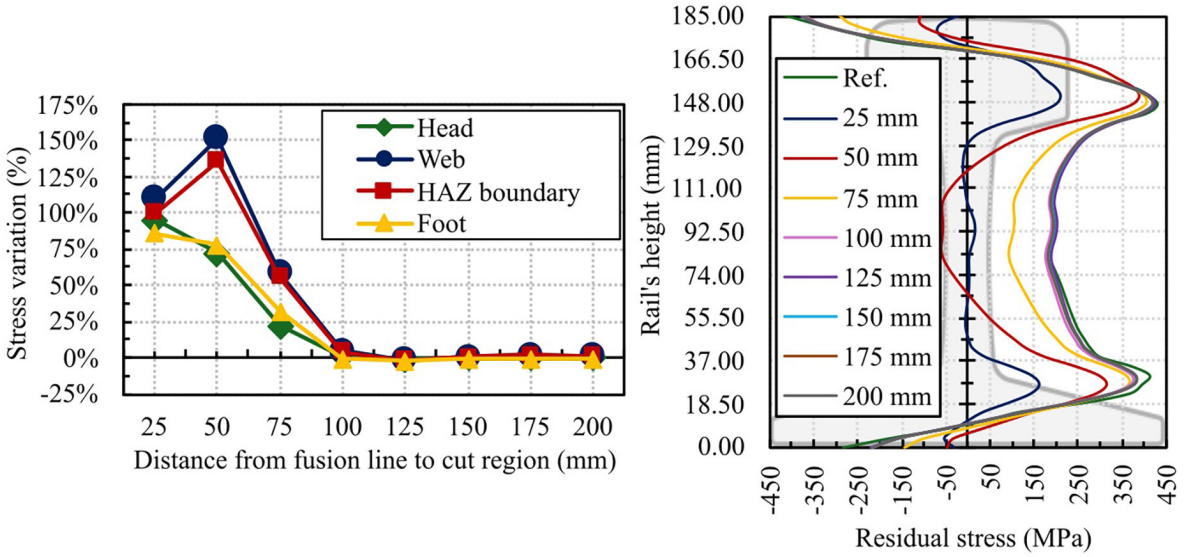

Figure 12: Longitudinal residual stress (σ_z) variation a) in the measured positions and b) along the rail's height at the FL.

region in the cut at 50 mm, which also increased in relation to the reference stress. These are interesting results, which deserve to be further investigated in future analyses.

However, the most important contribution of this work is that the results show that for cuts with a distance starting at 150 mm from the fusion line, none of the stresses at the points analyzed in the weld region undergo changes. Significant variations only really occur from a distance of 75 mm.

This conclusion from the numerical results was corroborated by the experimental results shown for specimens with 2 m and 0.35 m, in which the magnitudes of the stresses at the same points evaluated numerically in the weld region did not have significant differences in most points.

Thus, it is shown that specimens with lengths starting at 300 mm (150 mm on each side of the fusion line) are a safe dimension for analyzing and measuring residual stresses in the weld region without concerns about significant modifications of the residual stresses in this region. This dimension for a TR-68 profile rail represents a mass of 20.4 kg, which makes the logistics of transportation, storage and handling easier for researchers to perform a greater number of experimental evaluations, providing statistically more reliable results.

6. ACKNOWLEDGMENTS

The authors thank NAAT — Núcleo Avançado de Análise de Tensões for providing the technological equipment necessary for the project's development and VALE for supplying the analyzed specimens.

7. REFERENCES

[1] FARHANGI, H., MOUSAVIZADEH, S.M., "Horizontal split-web fractures of flash butt welded rails", In: *Proceedings of the 8th International Fracture Conference*, pp. 509–517, Istanbul, Turkey, 2007.

[2] FUJII, M., NAKANOWATARI, H., NARIAI, K., "Rail flash-butt welding technology", *JFE Technical Report*, v. 20, pp. 159–163, 2015.

[3] PANG, Y., GRILLI, N., SU, H., *et al.*, "Experimental investigation on microstructures and mechanical properties of PG4 flash-butt rail welds", *Engineering Failure Analysis*, v. 141, pp. 106650, 2022. doi: http://doi.org/10.1016/j.engfailanal.2022.106650.

[4] FICK, W.T., "Medição e análise de tensões residuais geradas na soldagem FBW de trilhos", M.Sc. Thesis, Universidade Federal do Pará, Belém, Pará, 2021.

[5] LI, Y., CHEN, J., WANG, J., *et al.*, "Study on the effect of residual stresses on fatigue crack initiation in rails", *International Journal of Fatigue*, v. 139, pp. 105750, 2020. doi: http://doi.org/10.1016/j.ijfatigue.2020.105750.

[6] LO, K.H., MUMMERY, P., BUTTLE, D.J., "Characterization of residual principal stresses and their implications on failure of railway rails", *Engineering Failure Analysis*, v. 17, n. 6, pp. 1273–1284, 2010. doi: http://doi.org/10.1016/j.engfailanal.2010.03.001.

[7] THADSOONGNOEN, K., HASAP, A., NORAPHAIPHIPAKSA, N., *et al.*, "Numerical investigation of residual stress formation mechanisms in flash-butt welded rail", *Metals*, v. 13, n. 8, pp. 1359, 2023. doi: http://doi.org/10.3390/met13081359.

[8] GHAZANFARI, M., TEHRANI, P.H., "Investigation of residual stress and optimization of welding process parameters to decrease tensile residual stress in the flash butt welded UIC60 rail", *Mechanics Based Design of Structures and Machines*, v. 50, n. 5, pp. 1580–1594, 2022. doi: http://doi.org/10.1080/15397734.2020.1756845.

[9] OLIVEIRA, B.S.D., RODRIGUES, L.A.S., COSTA, E.S., *et al.*, "X-ray diffraction analysis of residual stresses in the premium rails welded by flash butt process", *Soldagem e Inspeção*, v. 25, pp. e2529, 2020. http://doi.org/10.1590/0104-9224/si25.29.

[10] MANSOURI, D., SENDUR, P., YAPICI, G.G., "Fatigue characteristics of continuous welded rails and the effect of residual stress on fatigue-ratchetting interaction", *Mechanics of Advanced Materials and Structures*, v. 27, n. 6, pp. 473–480, 2020. doi: http://doi.org/10.1080/15376494.2018.1480820.

[11] CASTRO, M.M.D., "Análise numérica e experimental de tensões residuais geradas em trilhos premium e super-premium soldados pelo processo FBW", M.Sc. Thesis, Universidade Federal do Pará, Belém, Pará, 2025.

[12] CAI, Z., NAWAFUNE, M., MA, N., *et al.*, "Residual stresses in flash butt welded rail", *Transactions of JWRI*, v. 40, n. 1, pp. 79–87, 2011. doi: https://doi.org/10.18910/4606

[13] MA, N., CAI, Z., HUANG, H., *et al.*, "Investigation of welding residual stress in flash-butt joint of U71Mn rail steel by numerical simulation and experiment", *Materials & Design*, v. 88, pp. 1296–1309, 2015. doi: http://doi.org/10.1016/j.matdes.2015.08.124.

[14] TAWFIK, D., MUTTON, P.J., CHIU, W.K., "Experimental and numerical investigations: alleviating tensile residual stresses in flash-butt welds by localized rapid post-weld heat treatment", *Journal of Materials Processing Technology*, v. 196, n. 1-3, pp. 279–291, 2008. doi: http://doi.org/10.1016/j.jmatprotec.2007.05.055.

[15] ALVES, L.H.D., PEREIRA, H.B., ECHEVERRI, E.A.A., *et al.*, "Influence of rail metallurgy and welding parameterization on the quality of flash butt welds done with mobile equipment", *Materials Research*, v. 27, pp. e20230566, 2024. doi: http://doi.org/10.1590/1980-5373-mr-2023-0566.

[16] RODRIGUES, L.D., FREIRE, J.L., VIEIRA, R.D., " Desenvolvimento e avaliação experimental de uma nova técnica para medição de tensões residuais", *Matéria*, v. 16, pp. 842–856, 2011. doi: http://doi.org/10.1590/S1517-70762011000400006.

[17] AMERICAN SOCIETY FOR TESTING AND MATERIALS, *E 837-13A: Standard Test Method for Determining Residual Stresses by the Hole-Drilling Strain-Gage Method*, West Conshohocken, ASTM, 2013.

[18] AMERICAN RAILWAY ENGINEERING AND MAINTENANCE-OF-WAY ASSOCIATION, "Rail", In: American Railway Engineering and Maintenance-of-Way Association (ed.), Manual for Railway Engineering, chapter 4, Lanham (MD), AREMA, p. 1312, 2011.